

Investigation on lithium ion battery equivalent circuit models for dynamic load profiles

Bansi L. Bairwa¹ | Kapil Pareek¹  | Santosh kumar Hampannavar²

¹Centre for Energy and Environment,
Malaviya National Institute of
Technology, Jaipur, India

²School of Electrical and Electronics
Engineering, REVA University,
Bengaluru, India

Correspondence

Kapil Pareek, Centre for Energy and
Environment, Malaviya National Institute
of Technology, Jaipur 302017, India.
Email: kapil.cee@mnit.ac.in

Abstract

To achieve accurate prediction of the nonlinear behavior of lithium-ion battery, parameters of the lithium-ion battery model play a key role for dynamic performance, hence the parameters of the investigated battery model have been estimated. In this work, the electrical equivalent circuit (ECM) models have been used to simulate INR18650-20R lithium-ion battery response at 0°C, 25°C, and 45°C, respectively. The ECM model parameters are estimated using incremental open-circuit voltage (OCV) profile and Trust-Region Reflective algorithm by the Non-Linear Least Squares method. The estimated parameters of the ECM model experimentally validated using independent dynamic current profiles including Dynamic Stress Test (DST), Federal urban driving schedule (FUDS), Beijing Dynamic Stress test (BJDST), and US06 at 0°C, 25°C, and 45°C, respectively. Coulomb-counting based algorithms are implemented for model-based online SoC estimation. The investigated ECM model with three parallel RC branches exhibits accuracy below 1.8% for different temperature levels and seems suitable to capture the nonlinear dynamics of lithium-ion batteries for EV application. It is confirmed that the errors resulting from the investigated ECM model are significantly reduced comparatively existing published models.

KEY WORDS

electric vehicle, electrical equivalent circuit model, energy storage, lithium-ion battery, state of charge

1 | INTRODUCTION

Battery modeling is very crucial to design and investigate the battery-operated drive train of electric vehicles. The battery models are being used for battery state estimation, optimization, simulation, and algorithm development for the battery management system BMS.^{1–4} Numerous battery modeling methods have been explored extensively in literature based on their accuracy and complexity. The motivation behind the work is to propose a lithium-ion battery model, that can predict battery behavior under dynamic load conditions.^{5–9}

From the published literature it has been found that battery models are categorized into four types.¹⁰ The first type of model is data-driven models (extreme learning machine model, support vector machine model, and neural network),¹¹ the second type of models is empirical models (Nernst model, Unnewehr universal model, shepherd model, zero state hysteresis model, enhanced self-correction model),¹² the third type of model is electrochemical models (single particle model and pseudo-2D model), and the fourth type of models is equivalent circuit models (Thevenin model, dual-polarization model, PNGV model, Rint Model,

NRC model) as per different levels of interpretation of battery behavior.¹³⁻¹⁶

The investigated models are based on the NRC (number of RC branches) equivalent circuit model. In published literature it has been found that increasing order of ECM, makes the system complex and inappropriate for parameter identification but the accuracy increases with higher order. The investigated models are considered for experimental investigation with identified parameters. The equivalent circuit models are relatively preferred due to their simplicity, easy to implement and less complexity.¹⁷⁻²⁰ The equivalent circuit models can be used to estimate non-linear behavior of battery and parametrization of model parameters which depend upon temperature, SoC, state of health (SOH), and c-rate (amp). These dependencies vary as per battery's chemistry and manufacture. Battery models also include algorithms for SoC estimation. There are different battery equivalent circuit models have been reported with varying resistor-capacitor blocks. The accuracy of the battery equivalent circuit models increases with RC blocks, however, the higher order of RC blocks leads to high complexity.^{5,21-23} The tradeoff could be 3RC blocks which might provide a better balance of accuracy and complexity of the model. The reported battery models are generally validated with experimental battery data which are not realistic profiles of electric vehicles. It is important to consider different dynamic current profiles for validation including Dynamic Stress Test (DST),²⁴ Federal urban driving schedule (FUDS),²⁵ and Beijing Dynamic Stress test (BJDST),²⁶ etc. Apart from this, regarding online SoC estimation, OCV-SoC mapping, and the effect of

temperature have not been widely evaluated for so far. It is very important to compare their effect as there may be a large error during online SoC estimation.^{5,8,27-34} Based on the above-discussed approach, in this paper, a three-branch equivalent circuit model (ECM) is investigated to estimate the non-linear behavior of INR18650-20R (LiNiMnCoO_2) lithium-ion battery.³⁵⁻³⁷ The battery model is validated with dynamic current profiles which include regenerative braking. Also, the temperature dependency of OCV-SoC curves on online SoC estimation is presented.³⁸⁻⁴⁵ The contributions made here have wide applicability in the battery behavior for EV application.^{6,9,23,30,38,39,46-60}

2 | METHODOLOGY

The methodology section is divided into three subparts: (a) Li-NMC single-cell model; (b) Validation; and (c) Drive Cycle test. During the first part, state of charge (SoC) vs open-circuit voltage (OCV) mapping, ECM modeling and parameter estimation were performed. In the second part, the developed model was validated using experimental data and in the third part, the model was simulated for electric vehicle drive cycle test profiles at different temperature. Figure 1 shows the methodology and Figure 2A,B shows the experimental set up for lithium-ion battery INR18650-20R with help of DC programmable load and Cadex C8000 battery tester and environmental chamber. The dynamic load profiles experimental data were taken from Centre for Advanced Life Cycle Engineering, University of Maryland for validation of the ECM models.¹⁹

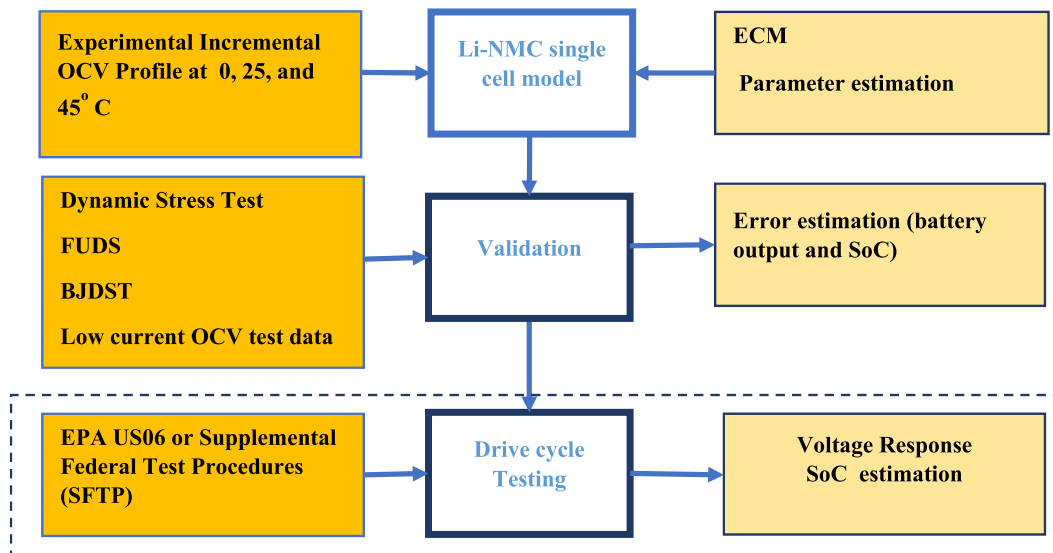


FIGURE 1 Methodology

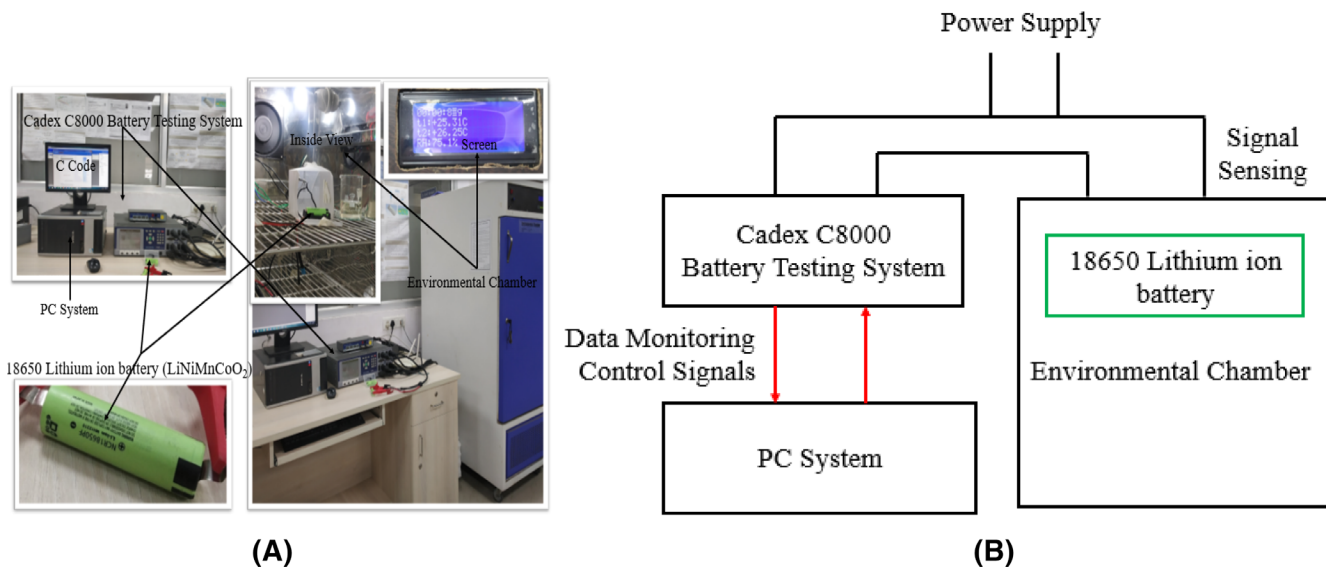
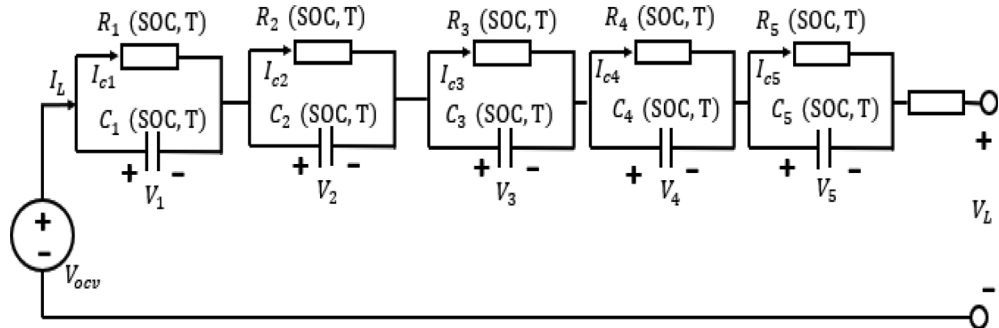


FIGURE 2 A, Experimental set up for lithium-ion battery; B, Testing layout

FIGURE 3 Equivalent circuit model of a lithium-ion battery



2.1 | Battery equivalent circuit model

An improved 1RC to 5RC electrical equivalent circuit models (ECM) were used to predict the nonlinear behavior of the Lithium-ion battery.

The investigated models consist of three parts an ideal voltage source, an RC network that describes polarization characteristics of the cell, and internal resistance R_0 that represents the ohmic losses. Figure 3 represents five RC branch equivalent circuit model consisting of 5 parallel RC branches, an ideal voltage source, and R_0 internal resistance. Each element of the equivalent circuit of Figure 3 is a function of SOC and temperature. The electrical behavior of the 5RC ECM model can be expressed by Equations (1-7).

$$V_L = V_{ocv} - V_1 - V_2 - V_3 - V_4 - V_5 - I_L * R_0 \quad (1)$$

$$\dot{V}_1 = -\frac{V_1}{R_1 C_1} + \frac{I_L}{C_1} \quad (2)$$

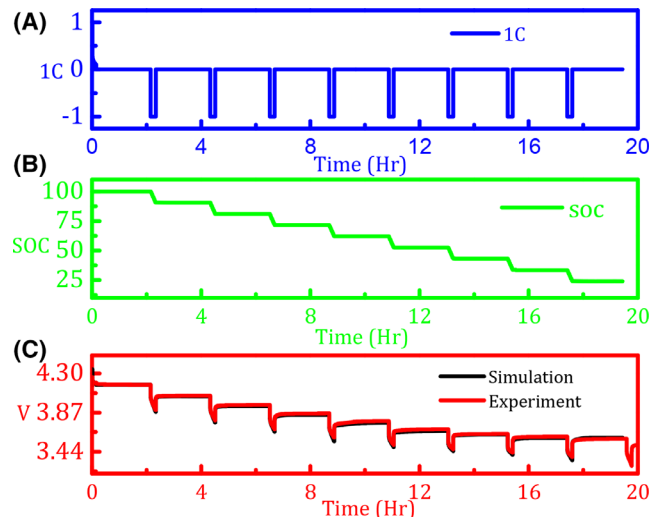


FIGURE 4 A, Incremental OCV load profile; B, SoC under parameter estimation; C, fitted curve for experimental and simulated voltage response

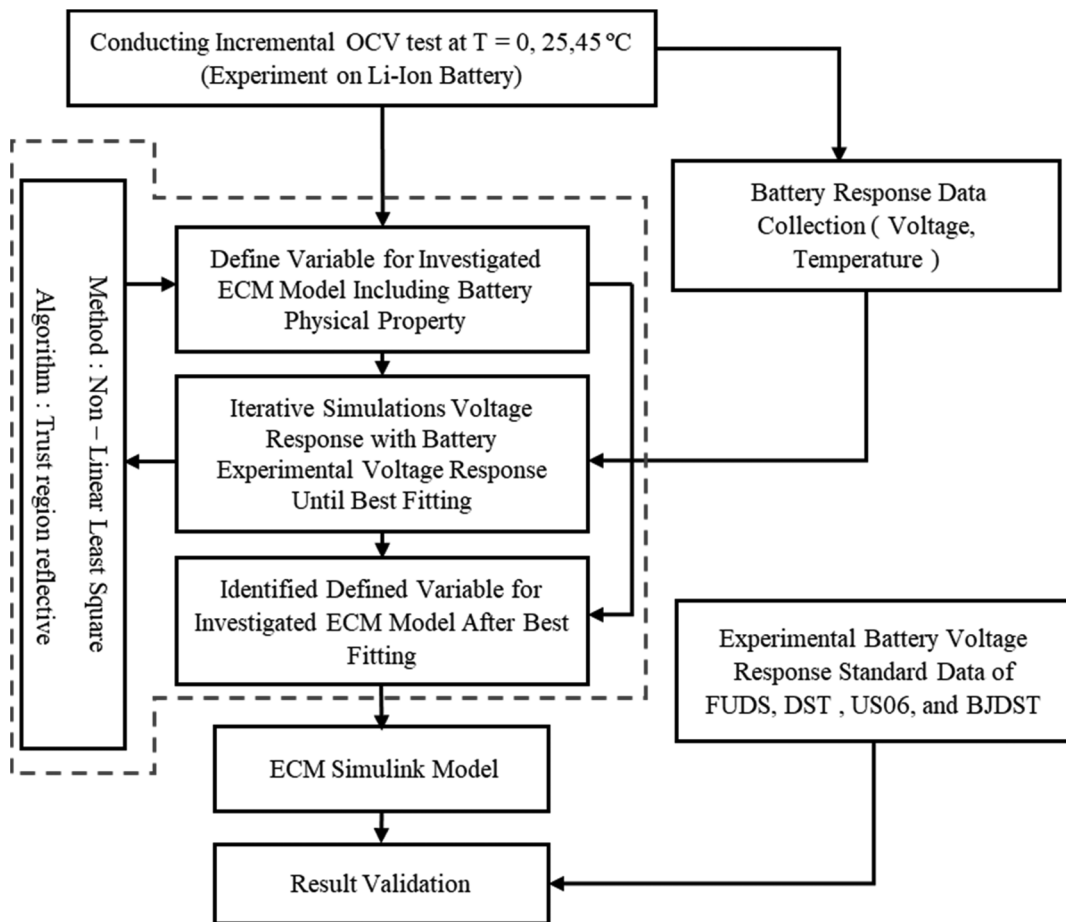


FIGURE 5 Flowchart for parameter estimation and validation of the investigated models

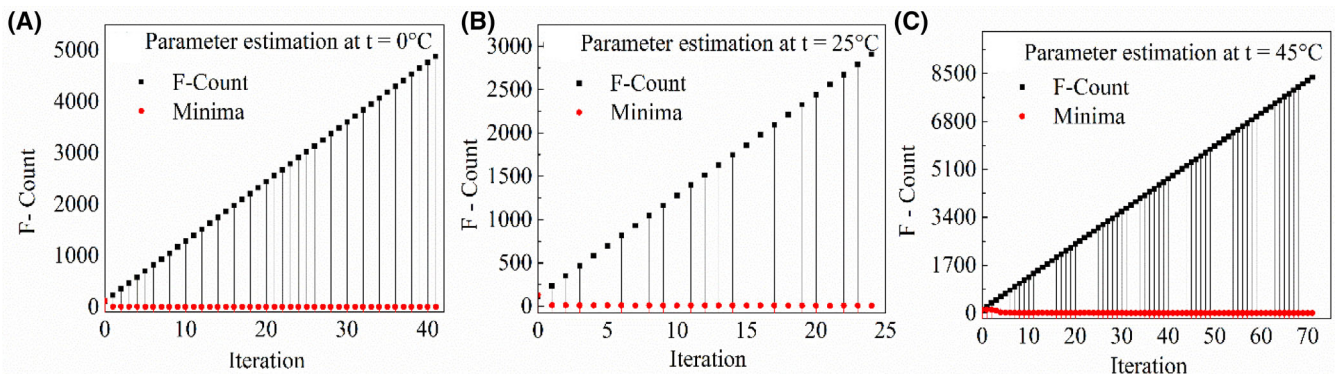


FIGURE 6 A-C, Parameter estimation lsqnnonlin solver response for pulse minimizing at $T = 0^\circ\text{C}$, 25°C , and 45°C , respectively for 1RC ECM

$$\dot{V}_2 = -\frac{V}{R_2 C_2} + \frac{I_L}{C_2} \quad (3)$$

$$\dot{V}_3 = -\frac{V_3}{R_3 C_3} + \frac{I_L}{C_3} \quad (4)$$

$$\dot{V}_4 = -\frac{V_4}{R_4 C_4} + \frac{I_L}{C_4} \quad (5)$$

$$\dot{V}_5 = -\frac{V_5}{R_5 C_5} + \frac{I_L}{C_5} \quad (6)$$

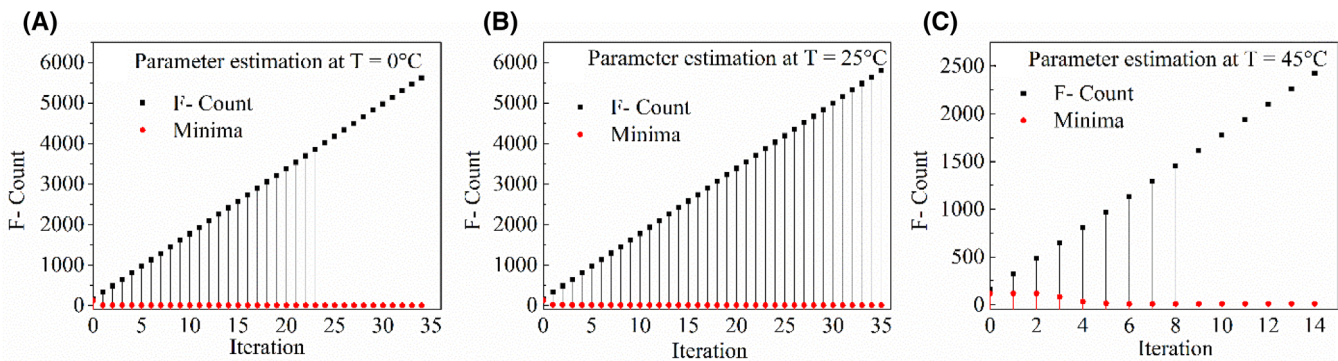


FIGURE 7 A-C, Parameter estimation lspnonlin solver response for pulse minimizing at $T = 0^\circ\text{C}$, 25°C , and 45°C , respectively for 2RC ECM

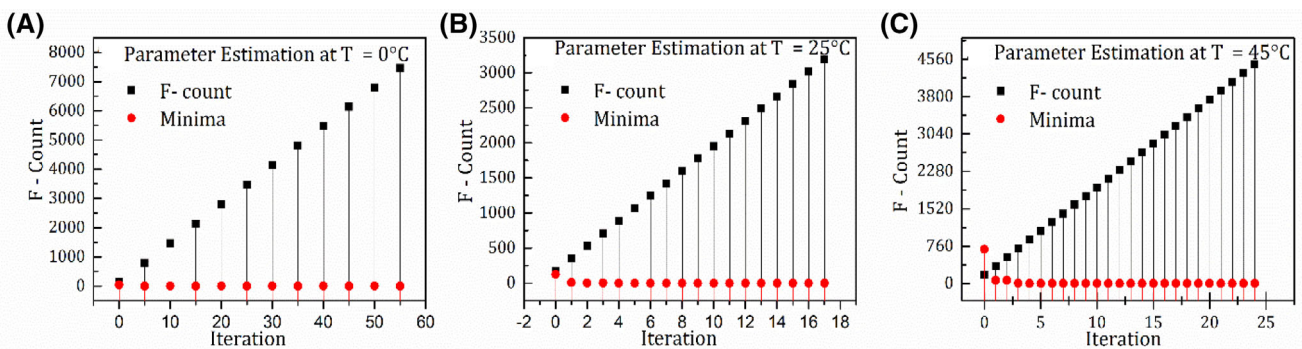


FIGURE 8 A-C, Parameter estimation lspnonlin solver response for pulse minimizing at $T = 0^\circ\text{C}$, 25°C , and 45°C , respectively for 3RC ECM

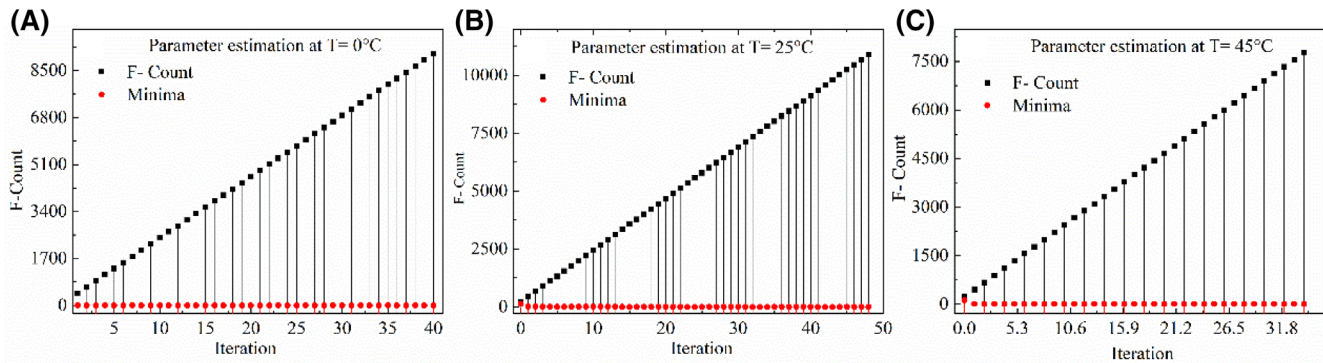


FIGURE 9 A-C, Parameter estimation lspnonlin solver response for pulse minimizing at $T = 0^\circ\text{C}$, 25°C , and 45°C , respectively for 4RC ECM

$$\begin{aligned} V_L &= V_{\text{ocv}} - \left(\int_0^t \frac{I_L}{C_1} - \frac{V_1}{R_1 C_1} \right) - \left(\int_0^t \frac{I_L}{C_2} - \frac{V_2}{R_2 C_2} \right) \\ &\quad - \left(\int_0^t \frac{I_L}{C_3} - \frac{V_3}{R_3 C_3} \right) - \left(\int_0^t \frac{I_L}{C_4} - \frac{V_4}{R_4 C_4} \right) - \left(\int_0^t \frac{I_L}{C_5} - \frac{V_5}{R_5 C_5} \right) - I_L R_0 \end{aligned} \quad (7)$$

where V_1 , V_2 , V_3 , V_4 , and V_5 are represented as a voltage across parallel RC branches. V_{ocv} is open-circuit voltage, R_0 internal resistances, R_1 , R_2 , R_3 , R_4 , R_5 , and C_1 , C_2 ,

C_3 , C_4 , C_5 are branches resistance and capacitance, respectively.

The Cells inside temperature can be computed by solving the heat Equations (8) and (9).

$$C_t \frac{dT}{dt} = \frac{T - T_a}{R_T} + P_s \quad (8)$$

after Laplace transformation

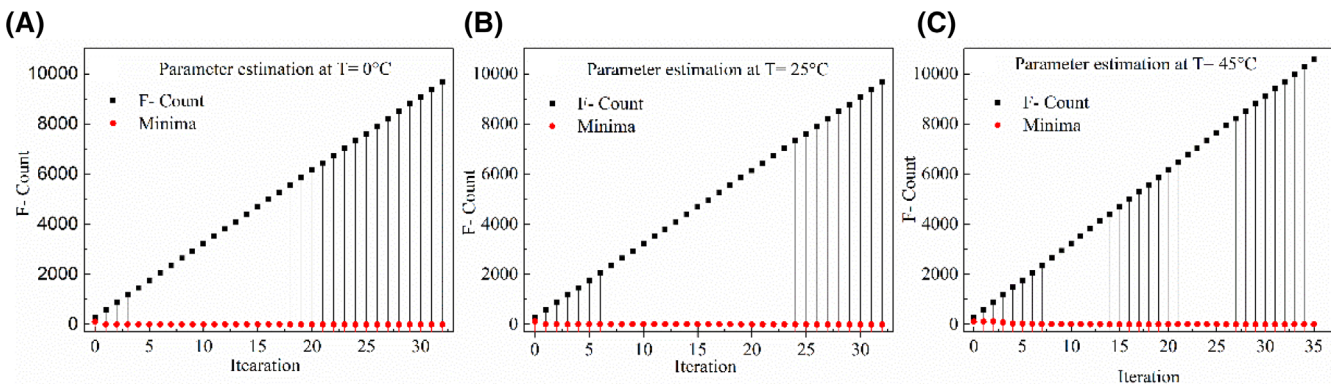


FIGURE 10 A-C, Parameter estimation lsqnnonlin solver response for pulse minimizing at $T = 0^\circ\text{C}$, 25°C , and 45°C , respectively for 5RC ECM

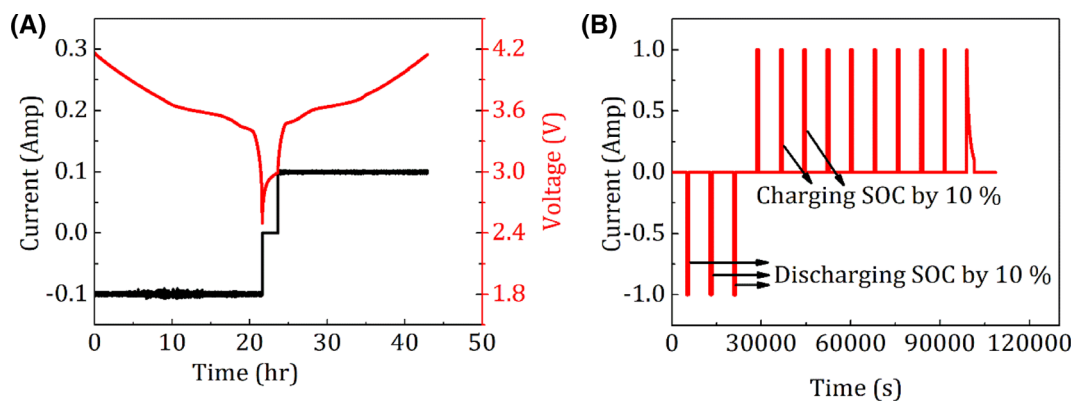


FIGURE 11 A, Low current open circuit voltage profile and B, Incremental open circuit voltage test profile

$$T(s) = \frac{P_s R_T + T_a}{1 + R_T C_T s} \quad (9)$$

where T is inside cell temperature ($^\circ\text{C}$), T_a is ambient temperature ($^\circ\text{C}$), R_T is convection resistance ($\text{W}^1 \text{M}^{-2} \text{K}^{-1}$), P_s is the power dissipated inside the cell (W), C_T is heat capacitance ($\text{J M}^{-3} \text{K}^{-1}$).

2.2 | Parameter estimation & algorithm

1RC to 5RC ECM parameters were investigated using an incremental OCV test profile (Figure 4) at three different temperatures (Figure 5). The trust-region reflective nonlinear least-squares algorithm was utilized with constraints to optimize the non-linear behavior of the battery.^{10,20} This nonlinear least-squares solver is faster than direct search methods because the subsequent iteration is based on first and second order derivatives which lead to an adjustment of the algorithm with minimal. Apart from this, the solver is used with bound-constrained and accurate initial conditions to

avoid suboptimal local minima in Figures 6 to 10. During parameter estimation, the incremental OCV profile was iteratively simulated and compared with experimental data. The circuit elements were parameterized using flexible lookup tables as time constants for 1RC ECM to 5RC ECM. Figure 12 represents only time constants lookup table for 5RC ECM model. Author has estimated lookup tables for 1RC to 5RC ECM time constants, the incremental OCV provides sufficient information for each pulse and the three temperature conditions were considered self-reliantly for parameter estimation. For each ECM element, lookup tables are based on 11x3 breakpoints as per SoC for temperature at 0°C , 25°C , and 45°C .

Figures 6 to 10 represents parameter estimation trust-region reflective nonlinear least square algorithm response for pulse minimizing with several iterations at temperature of 0°C , 25°C , and 45°C , respectively. In the Simulink Design Optimization toolbox, solver LSQNNONLIN (trust-region reflective nonlinear least square algorithm) was chosen for estimating the parameters because it is comparatively faster than direct search

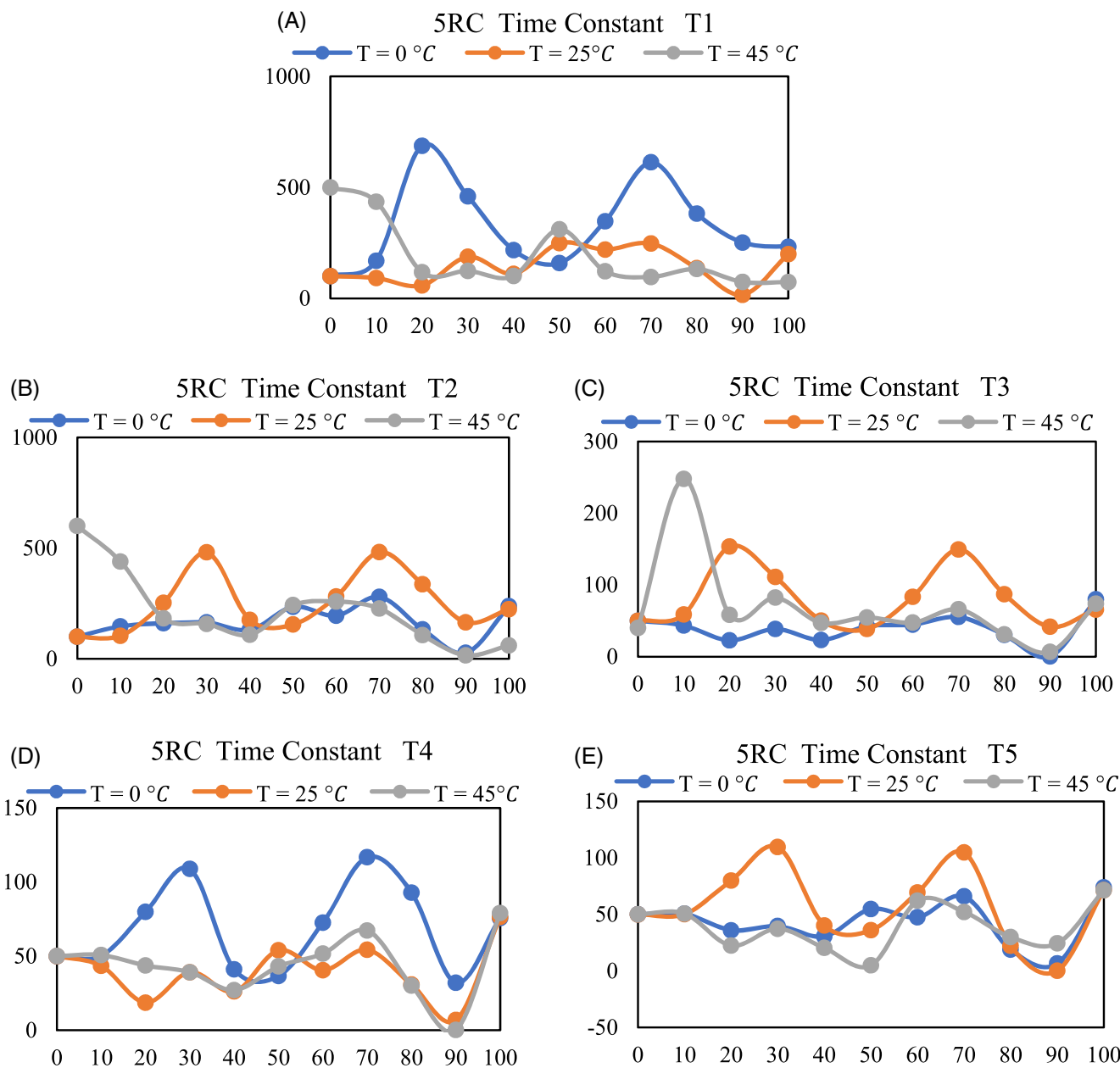


FIGURE 12 A-E, Time Constants at $T = 0^\circ\text{C}$, 25°C , and 45°C , for 5RC ECM model

methods such as PATTERNSEARCH. Error minimization is achieved as per Equation (10)

$$\text{err}(X_a(t), X_m(t)) = \min \quad (10)$$

where $X_m = (V_m, T_m)$ and $X_a = (V_a, T_a)$ are model and actual quantities respectively. Here X_m and X_a is a function of voltage and temperature, the load voltage V_L is the sum of voltage drop due to internal resistance and the number of branch voltage. The variable voltage drop across the number of RC branches is based on the time constants appears due the number of RC branches.

2.3 | SoC-OCV mapping

SoC-OCV curve was mapped with experimental battery test data. SoC-OCV mapping is a nonlinear monotonic function between SoC and OCV. This mapping is widely used in the battery management system for correcting SoC estimation which is carried out through different direct and indirect methods, such as Kalman filter, coulomb counting, fuzzy logic, adaptive filter-based methods.^{42,61-65} In low current open circuit voltage test, the battery is charged with 1C and then fully discharged with C/20 until cut-off voltage as per the datasheet. After that, the battery is charged with C/20

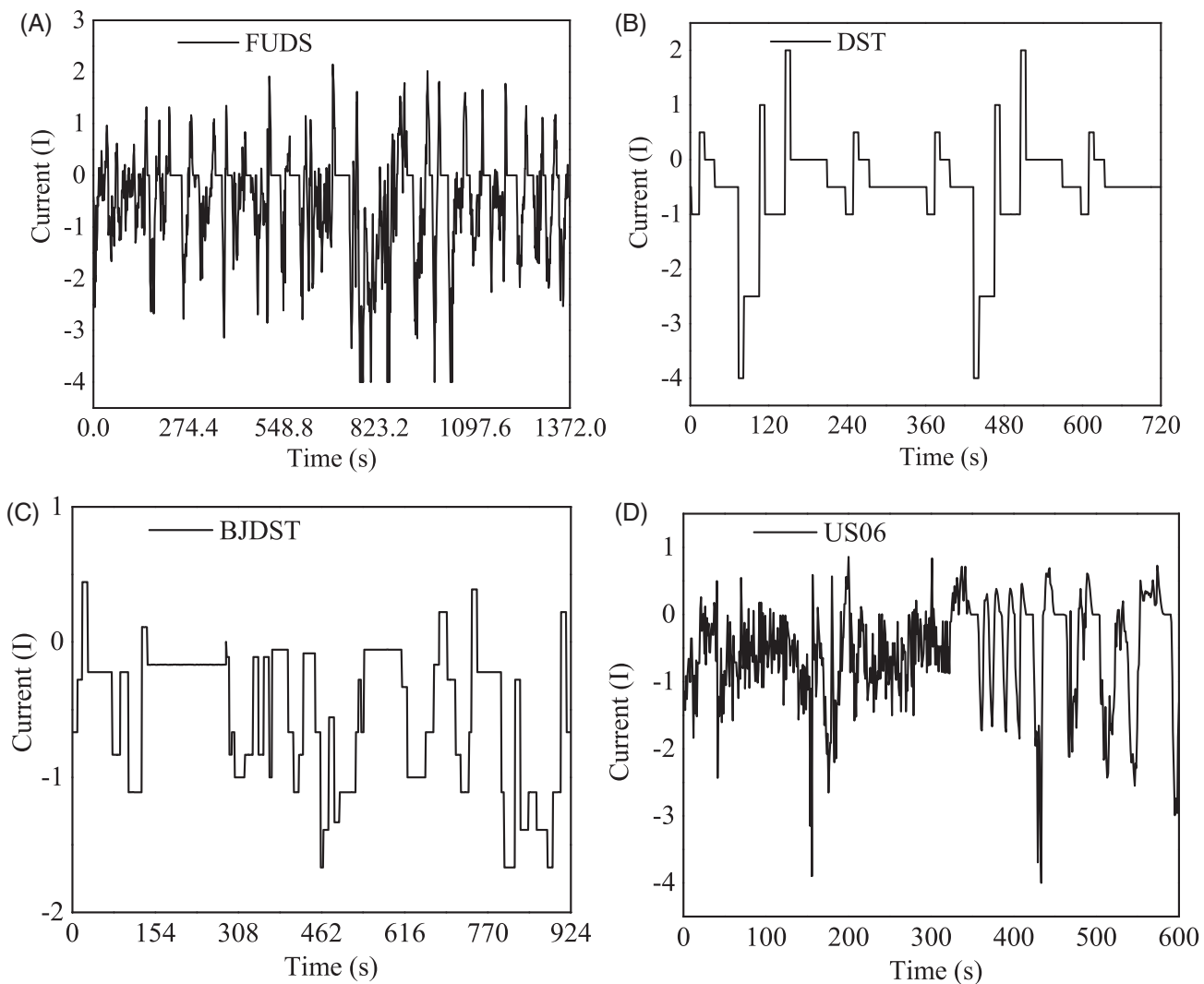


FIGURE 13 Dynamic load profiles

(Figure 11A). While in incremental OCV, the fully charged battery is discharged with lower pulse current-relaxation during at every 10% SoC and then charged with an upper pulse current (Figure 11B). The OCV–SoC mapping curve is obtained by averaging and a linear interpolation step.¹⁹

2.4 | Online SOC estimation

The Coulomb counting method was implemented to estimate SoC of the battery. The method estimates the SoC by discharging current and integrating the discharging current over time.⁴⁴ The calculation of SoC is based on Equation (5), where the SoC_0 represents the initial SoC, I_{bat} represents the current across the battery and, Q_{rated} is the nominal capacity of the battery. The method of applying for model-based SoC estimation has a closed-loop structure.^{20,35,66,67}

$$\text{SoC} = \text{SoC}_0 + \frac{\int_{t_0}^t I_{\text{bat}} \Delta t}{Q_{\text{rated}}} \quad (11)$$

2.5 | Estimated parameters

Figure 12 shows the result of the estimated parameters which constitute the look-up tables for the 5RC ECM models. Furthermore, it shows how the parameters are dependent on SoC levels and temperature. The range of SoC taken from deep discharge to fully charging condition assumed 100% SoC and breakpoints for SoC taken as 10% SoC increments at each breakpoint. Total 11 breakpoints taken for SoC and the estimated parameters value divided into three temperature ranges. Time constants for the ECM model calculated for each respective parallel RC branch. Time constants of the ECM model represent the internal behavior of the lithium-ion battery that is responsible for the losses that occur inside the battery.^{68–70} 1RC ECM

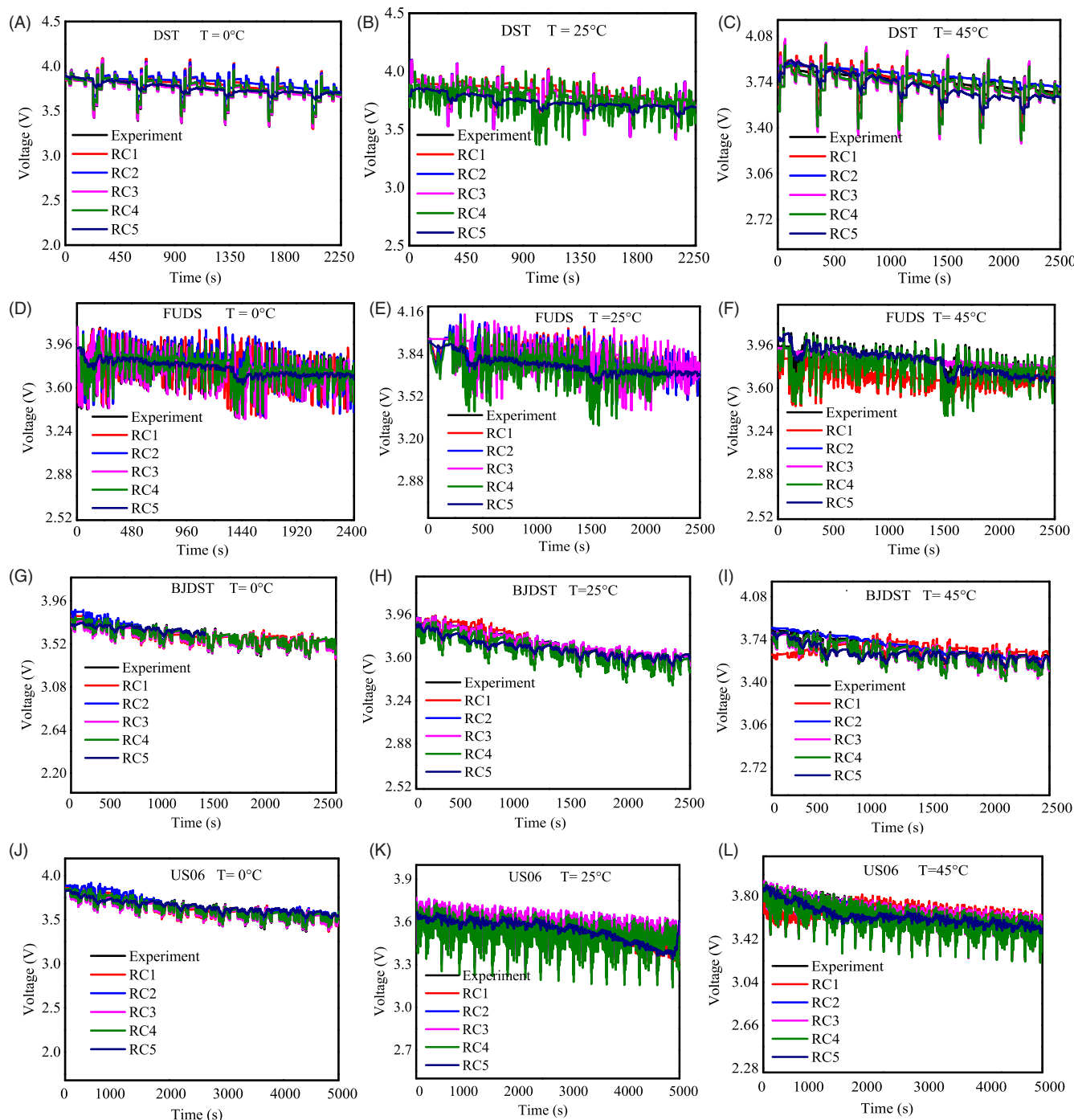


FIGURE 14 A-L, Experimental and simulated voltage response for DST, FUDS, BJDST, & US06 tests at 0°C, 25°C, and 45°C, respectively

model has one time constant, 2RC ECM model has two parallel branches so this model has two-time constants, the same this applied for remaining ECM models.

Different dynamic current profiles were selected to validate the model outcome and SoC estimation (Figure 13). These test profiles also take into account of regenerative charging of the battery. The time is taken to complete one test profile for DST, FUDS, US06, and

BJDST is 1180, 1372, 600, and 916 seconds, respectively. Dynamic stress test and federal urban drive schedule tests have been used to determine the Variable Power Discharge capacity of the lithium-ion battery.⁷¹ Dynamic current profiles (FUDS), US06, and (BJDST) are more complex than the Dynamic stress test in terms of the changing or discharging rate of the current.

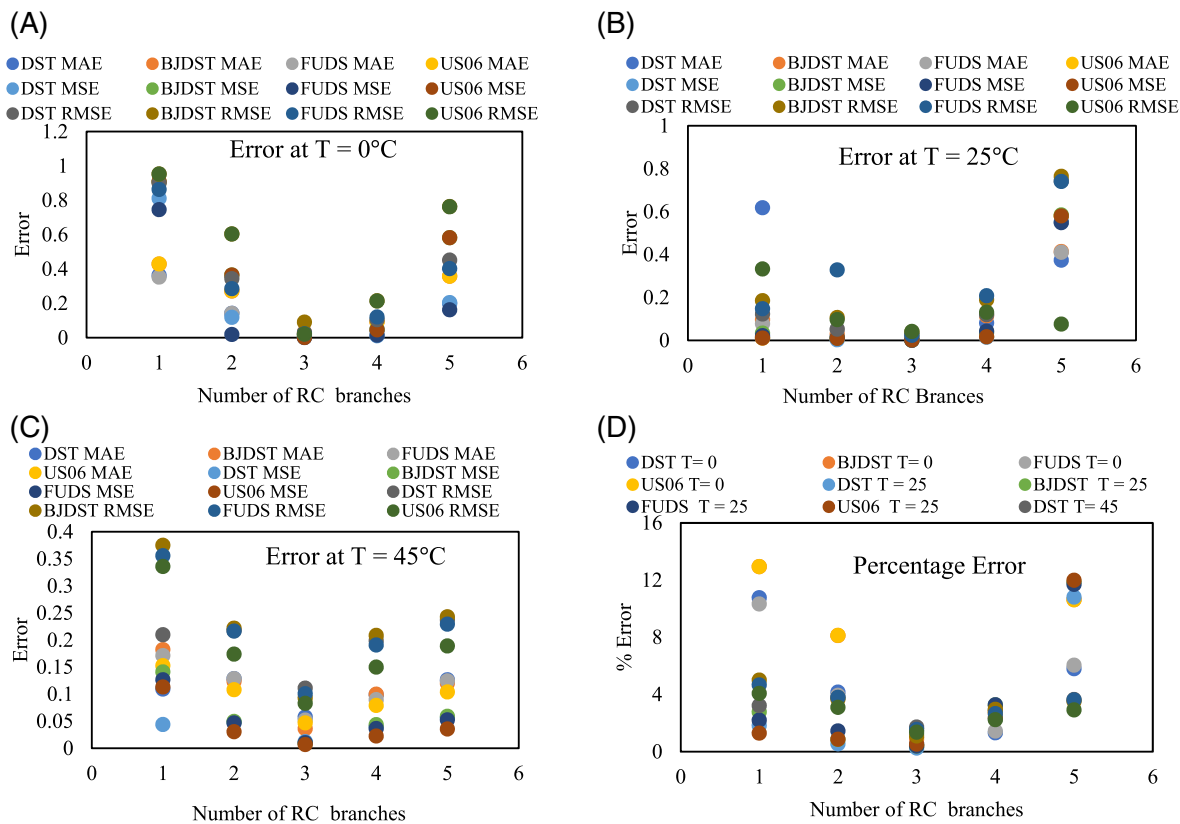


FIGURE 15 A-C, Represents MAD, MSE, and RMSE voltage errors for model voltage response at 0°C, 25°C, and 45°C respectively, panel D represents percentage error for 1RC to 5RC ECM voltage response

These repeated test profiles were applied to predict battery behavior. ECM model estimated voltage and SoC data were validated using experimental data mean absolute error (MAE), mean square error (MSE), root mean square error (RMSE), and mean absolute percentage error were calculated by Equations (12) to (15).^{31,72,73}

$$\text{MAE} = \sum_{k=1}^n |a_k - b_k| \quad (12)$$

$$\text{MSE} = \frac{1}{n} \sum_{i=1}^n (a_k - b_k)^2 \quad (13)$$

$$\text{RMSE} = \sqrt{\frac{1}{n} \sum_{i=1}^n (a_k - b_k)^2} \quad (14)$$

$$\text{MAPE} = \left(\frac{1}{n} \sum_{k=1}^n \frac{|a_k - b_k|}{a_k} \right) * 100 \quad (15)$$

ECM ranging from 1 RC to 5RC. Furthermore, the model outcomes are also validated using experimental data at three different temperatures. It can be noticed that, the outcome of the 3RC ECM model shows relatively good agreement with experimental data.

To further investigate, errors analysis has been performed and shown in Figure 15. The mean absolute error (MAE), mean square error (MSE), root mean square error (RMSE), and Mean Absolute Percentage Error were calculated for all ECM models.

Notably, the RMSE and MAE errors are less for 3 RC ECM for different temperatures, confirming that three branch ECM models can effectively simulate the battery profiles at a wide range of temperatures.

Validation for the SoC estimation is shown in Figure 16A-L for 1RC ECM to 5RC ECM. The Figure shows the comparison between estimated SoC to true SoC. Here true SoC is identified by the ampere-hours SoC estimation method. SoC range is taken as minimum SoC level “Deep Discharge (100% DoD)” to the maximum level of the SoC that is considered as 100% SoC for the investigation. The estimation of the SoC is estimated after the load profile is applied as a load for the investigated models. The model response is predicted as voltage and the SoC level. The load profile for the model SoC estimation is taken

3 | RESULTS AND DISCUSSION

Figure 14 shows the voltage response of investigated battery models for different dynamic current profiles and

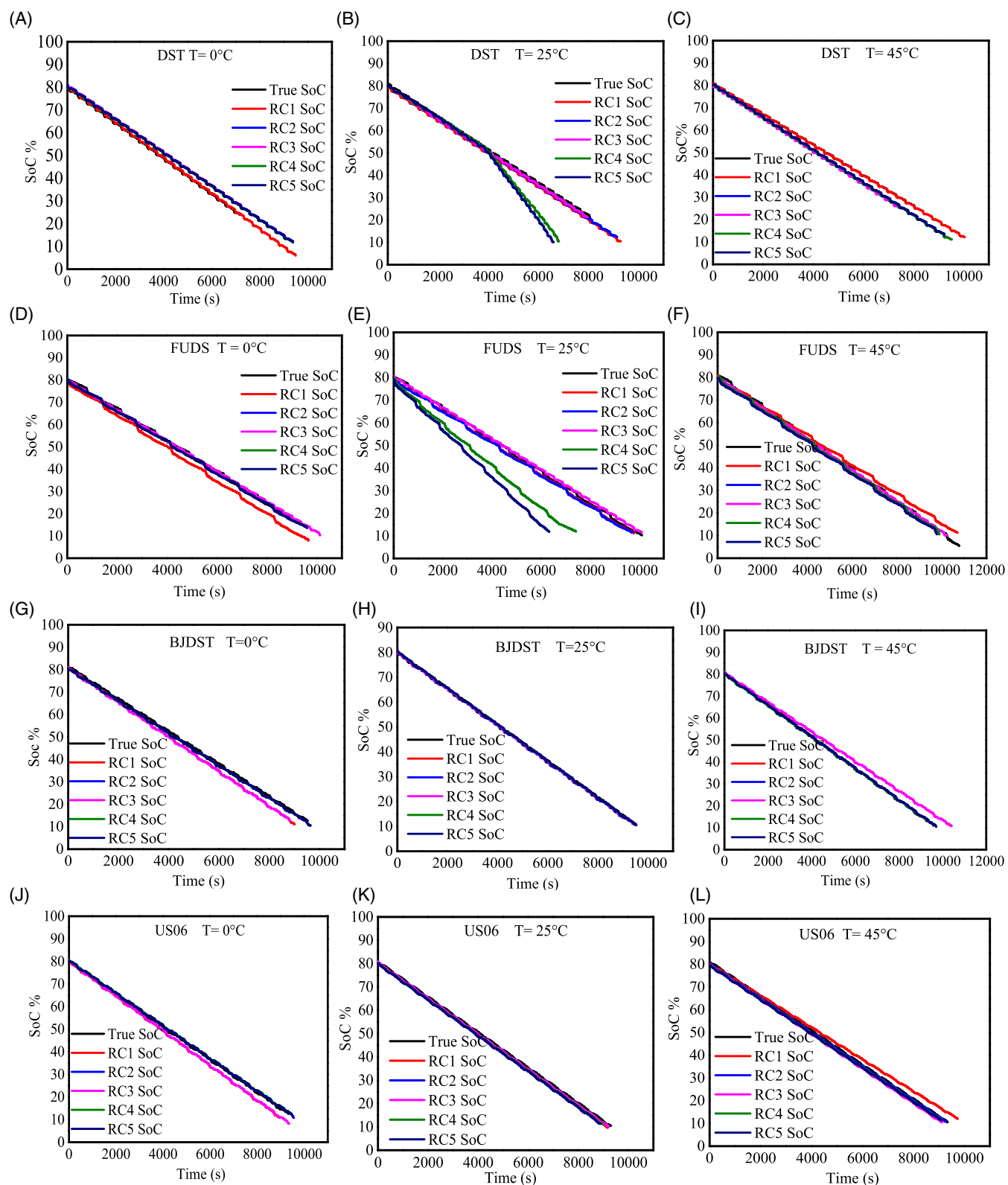


FIGURE 16 A-L, DST, FUDS, BJDST, and EPA/US06 drive cycles, SoC prediction for 1RC ECM to 5RC ECM at 0°C , 25°C , and 45°C , respectively

DST, FUDS, BJDST, and US06 that have been discussed in the previous section. The last part of this section is error analysis. Error is predicted from the

true SoC and the estimated SoC difference. Three types of error, MAD, MSE, and RMSE have been calculated in this section.

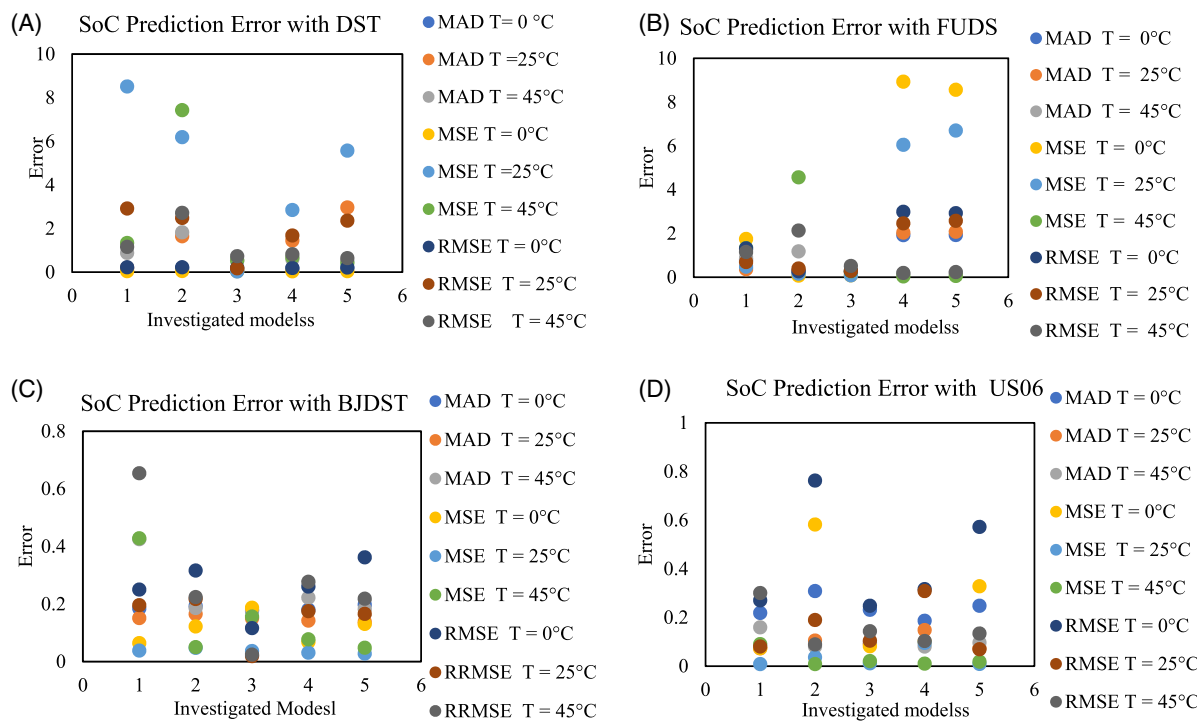


FIGURE 17 DST, FUDS, BJDST, & US06 drive cycles, SoC prediction error for 1RC ECM to 5RC ECM at 0°C, 25°C, and 45°C, respectively

Figure 16A-D compare the results of estimated SoC for FUDS, BJDST, and US06 profiles from the online estimator at 0°C temperature. Figure 17 shows SoC estimation errors of online SoC estimator 1 from the true SoC for the temperature 0°C, 25°C, and 45°C, respectively. The data of minimum SoC condition has been neglected from 0% to 10% SoC, the battery is usually operated from 10% to 90% state of charging condition.

4 | CONCLUSIONS

The study presents the investigation on 1RC to 5RC ECM modeling approach for Lithium-ion battery Equivalent circuit modeling of lithium-ion battery for electric vehicle application using incremental open circuit test profile at three temperature conditions. Validation of the model using experimental variable power test profile including a drive cycle test. Investigation of accuracy of 1RC to 5RC models. 3RC ECM model shows good accuracy and exhibits a minimum error of up to 1.8%. It has been investigated that the ECM model with three RC branch offers the best trade-off between accuracy and parameterization effort. Detailed analysis of predicting SoC error with different dynamic load profiles.

Three branches equivalent circuit cell model including cell thermal dynamics is presented. The ECM model parameters are obtained using incremental OCV based

pulse discharge experimental to generate lookup tables with cell temperature and SoC as independent variables. The equivalent circuit with a voltage source, a series resistor, and three parallel RC elements are adequate to capture the dynamics of a 18 650 Lithium-ion battery (LiNiMnCoO_2) having a nominal capacity of 2 Ah at different temperature conditions. The trust-region reflective nonlinear least-squares algorithm has been utilized for the parameter estimation. The model was validated using different dynamic current profiles at 0°C, 25°C, and 45°C, which showed cell voltage accuracy within 1.8%. The model used Coulomb-counting based algorithms for online SoC estimation which shows accuracy within 3% from the true SoC data at 0°C, 25°C, and 45°C. The results show that the three-branch equivalent circuit cell model is seeming to be suitable to capture the nonlinear dynamics of the lithium-ion battery for EV application.

ACKNOWLEDGMENTS

The authors gratefully acknowledge to Centre for Advanced Life Cycle Engineering, University of Maryland for the experimental battery test data. Testing facilities were available at the Centre for Energy & Environment, Malaviya National Institute of Technology Jaipur.

CONFLICT OF INTEREST

The authors declare no potential conflict of interest.

DATA AVAILABILITY STATEMENT

Data are included in the manuscript.

ORCID

Kapil Pareek  <https://orcid.org/0000-0001-7534-2804>

REFERENCES

1. Zhao Y, Stein P, Bai Y, al-Siraj M, Yang Y, Xu BX. A review on modeling of electro-chemo-mechanics in lithium-ion batteries. *J Power Sources*. 2019;413:259-283.
2. Bairwa BL, Soni A, Pareek K. Higher order equivalent circuit model analysis of lithium ion battery for electric vehicle. *AIP Conf Proc*. 2020;2294(1):40011.
3. Garg A, Peng X, le MLP, Pareek K, Chin CMM. Design and analysis of capacity models for lithium-ion battery. *Measurement*. 2018;120:114-120.
4. Rohan R, Pareek K, Chen Z, Cheng H. A pre-lithiated phloroglucinol based 3D porous framework as a single ion conducting electrolyte for lithium ion batteries. *RSC Adv*. 2016;6 (58):53140-53147.
5. Hussein AA. Adaptive artificial neural network-based models for instantaneous power estimation enhancement in electric Vehicles' Li-ion batteries. *IEEE Trans Ind Appl*. 2019;55(1): 840-849.
6. Li J, Wang D, Pecht M. An electrochemical model for high C-rate conditions in lithium-ion batteries. *J Power Sources*. 2019; 436:226885.
7. Nagode M, Gosar A, Sweeney CA, Jaguemont J, van Mierlo J, Šeruga D. Mechanistic modelling of cyclic voltage-capacity response for lithium-ion batteries. *Energy*. 2019;186:115791.
8. Gholizadeh M, Yazdizadeh A. State of charge estimation of a lithium-ion battery using robust non-linear observer approach. *IET Electr Syst Transport*. 2019;9(1):1-7.
9. Tremblay O, Dessaint L-A. Experimental validation of a battery dynamic model for EV applications. *World Electr Veh J*. 2009;3 (2):289-298. <https://doi.org/10.3390/wevj3020289>.
10. Xiong R, He H, Guo H, Ding Y. Modeling for lithium-ion battery used in electric vehicles. *Procedia Eng*. 2011;15:2869-2874.
11. Lipu MSH, Hannan MA, Hussain A, Saad MH, Ayob A, Uddin MN. Extreme learning machine model for state-of-charge estimation of lithium-ion battery using gravitational search algorithm. *IEEE Trans Ind Appl*. 2019;55(4):4225-4234.
12. Samadani E, Farhad S, Scott W, et al. Empirical modeling of lithium-ion batteries based on electrochemical impedance spectroscopy tests. *Electrochim Acta*. 2015;160:169-177.
13. Huo W, He H, Sun F. Electrochemical-thermal modeling for a ternary lithium ion battery during discharging and driving cycle testing. *RSC Adv*. 2015;5(71):57599-57607.
14. Klein R, Chaturvedi NA, Christensen J, Ahmed J, Findeisen R, Kojic A. Electrochemical model based observer Design for a Lithium-ion Battery. *IEEE Trans Control Syst Technol*. 2013;21 (2):289-301.
15. Jackey R, Saginaw M, Sanghvi P, Gazzarri J. Battery model parameter estimation using a layered technique: an example using a lithium iron phosphate cell. *SAE Int*. 2013. <https://doi.org/10.4271/2013-01-1547>.
16. Huria T, Ceraolo M, Gazzarri J, Jackey R. Simplified extended Kalman filter observer for SOC estimation of commercial power-oriented LFP lithium battery cells. *SAE Int*. 2013. <https://doi.org/10.4271/2013-01-1544>.
17. Hu X, Sun F, Zou Y, Peng H. Online estimation of an electric vehicle lithium-ion battery using recursive least squares with forgetting. Paper presented at: Proceedings of the 2011 American Control Conference; 2011.
18. Letcher TM. Preface. In: Letcher TM, ed. *Storing Energy*. Oxford: Elsevier; 2016:xxi-xxiv.
19. Zheng F, Xing Y, Jiang J, Sun B, Kim J, Pecht M. Influence of different open circuit voltage tests on state of charge online estimation for lithium-ion batteries. *Appl Energy*. 2016;183:513-525.
20. Kim T, Adhikaree A, Pandey R, et al. An on-board model-based condition monitoring for lithium-ion batteries. *IEEE Trans Ind Appl*. 2019;55(2):1835-1843.
21. Meng J, Luo G, Ricco M, Swierczynski M, Stroe DI, Teodorescu R. Overview of lithium-ion battery modeling methods for state-of-charge estimation in electrical vehicles. *Appl Sci*. 2018;8(5):659.
22. Zhao R, Kollmeyer PJ, Lorenz RD, Jahns TM. A compact methodology via a recurrent neural network for accurate equivalent circuit type modeling of lithium-ion batteries. *IEEE Trans Ind Appl*. 2019;55(2):1922-1931.
23. Dvorak D, Bauml T, Holzinger A, Popp H. A comprehensive algorithm for estimating lithium-ion battery parameters from measurements. *IEEE Trans Sustain Energy*. 2018;9(2):771-779.
24. Ding X, Zhang D, Cheng J, Wang B, Luk PCK. An improved Thevenin model of lithium-ion battery with high accuracy for electric vehicles. *Appl Energy*. 2019;254:113615.
25. Lia GL, Li S. Physics-based CFD simulation of lithium-ion battery under the FUDS driving cycle. *Electrochim Soc*. 2015;64(33):1-14.
26. Linfeng Z, Jiang J, Wang Z, Zhao T, He T. Embedded implementation of SOC estimation based on the Luenberger observer technique. Paper presented at: 2014 IEEE Conference and Expo Transportation Electrification Asia-Pacific (ITEC Asia-Pacific); 2014.
27. Gao Y, Zhang X, Cheng Q, Guo B, Yang J. Classification and review of the charging strategies for commercial lithium-ion batteries. *IEEE Access*. 2019;7:43511-43524.
28. Redondo-Iglesias E, Venet P, Pelissier S. Efficiency degradation model of lithium-ion batteries for electric vehicles. *IEEE Trans Ind Appl*. 2019;55(2):1932-1940.
29. Cui, X, Panda, B, Chin, CMM, Sakundarini, N, Wang, C-T, Pareek, K. An application of evolutionary computation algorithm in multidisciplinary design optimization of battery packs for electric vehicle. *Energy Storage*. 2020;2:e158. <https://doi.org/10.1002/est.2158>
30. Lyu C, Song Y, Zheng J, et al. In situ monitoring of lithium-ion battery degradation using an electrochemical model. *Appl Energy*. 2019;250:685-696.
31. Brivio C, Musolino V, Merlo M, Ballif C. A physically-based electrical model for lithium-ion cells. *IEEE Trans Energy Conversion*. 2019;34(2):594-603.
32. Zhang K, Ma J, Zhao X, Zhang D, He Y. State of charge estimation for lithium battery based on adaptively weighting cubature particle filter. *IEEE Access*. 2019;7:166657-166666.
33. Wenwei W, Yiding L, Cheng L, Yuefeng S, Sheng Y. State of charge-dependent failure prediction model for cylindrical lithium-ion batteries under mechanical abuse. *Appl Energy*. 2019;251:113365.

34. Bai Y, Zhao Y, Liu W, Xu BX. Two-level modeling of lithium-ion batteries. *J Power Sources*. 2019;422:92-103.
35. Yu Q-Q, Xiong R, Wang LY, Lin C. A comparative study on open circuit voltage models for lithium-ion batteries. *Chin J Mech Eng*. 2018;31(1):65.
36. Hu X, Xiong R, Egardt B. Model-based dynamic power assessment of lithium-ion batteries considering different operating conditions. *IEEE Trans Ind Inform*. 2014;10(3):1948-1959.
37. von Lüders C, Keil J, Webersberger M, Jossen A. Modeling of lithium plating and lithium stripping in lithium-ion batteries. *J Power Sources*. 2019;414:41-47.
38. Jaguemont J, Boulon L, Dubé Y. Characterization and modeling of a hybrid-electric-vehicle lithium-ion battery pack at low temperatures. *IEEE Trans Veh Technol*. 2016;65(1):1-14.
39. Ahmad P. Development of Battery Hardware-In-the-Loop System Implemented with Reduced-Order Electrochemistry Li-Ion Battery Models (2014-01-1858). *Lithium Ion Batteries in Electric Drive Vehicles*. Warrendale, Pennsylvania: SAE; 2016:35-41.
40. Yang F, Xing Y, Wang D, Tsui KL. A comparative study of three model-based algorithms for estimating state-of-charge of lithium-ion batteries under a new combined dynamic loading profile. *Appl Energy*. 2016;164:387-399.
41. Hu X, Li SE, Yang Y. Advanced machine learning approach for lithium-ion battery state estimation in electric vehicles. *IEEE Trans Transport Electrificat*. 2016;2(2):140-149.
42. Shen J-N, Shen J-J, He Y-J, Ma Z-H. Accurate state of charge estimation with model mismatch for Li-ion batteries: a joint moving horizon estimation approach. *IEEE Trans Power Electron*. 2019;34(5):4329-4342.
43. Fang H, Wang Y, Sahinoglu Z, Wada T, Hara S. Adaptive estimation of state of charge for lithium-ion batteries. Paper presented at: 2013 American Control Conference; 2013.
44. Meng J, Luo G, Gao F. Lithium polymer battery state-of-charge estimation based on adaptive unscented Kalman filter and support vector machine. *IEEE Trans Power Electron*. 2016;31(3):2226-2238.
45. Hu X, Sun F, Zou Y. Estimation of state of charge of a lithium-ion battery pack for electric vehicles using an adaptive Luenberger observer. *Energies*. 2010;3(9):1586-1603. <https://doi.org/10.3390/en3091586>.
46. Dai H, Guo P, Wei X, Sun Z, Wang J. ANFIS (adaptive neuro-fuzzy inference system) based online SOC (state of charge) correction considering cell divergence for the EV (electric vehicle) traction batteries. *Energy*. 2015;80:350-360.
47. Kellner Q, Hosseinzadeh E, Chouchelamane G, Widanage WD, Marco J. Battery cycle life test development for high-performance electric vehicle applications. *J Energy Storage*. 2018;15:228-244.
48. Patnaik L, Praneeth AVJS, Williamson SS. A closed-loop constant-temperature constant-voltage charging technique to reduce charge time of lithium-ion batteries. *IEEE Trans Ind Electron*. 2019;66(2):1059-1067.
49. Merla Y, Wu B, Yufit V, Martinez-Botas RF, Offer GJ. An easy-to-parameterise physics-informed battery model and its application towards lithium-ion battery cell design, diagnosis, and degradation. *J Power Sources*. 2018;384:66-79.
50. Plett GL. Extended Kalman filtering for battery management systems of LiPB-based HEV battery packs: part 1. Background. *J Power Sources*. 2004;134(2):252-261.
51. Ma Z, Jiang J, Shi W, Zhang W, Mi CC. Investigation of path dependence in commercial lithium-ion cells for pure electric bus applications: aging mechanism identification. *J Power Sources*. 2015;274:29-40.
52. Mejdoubi AE, Chaoui H, Gualous H, Van Den Bossche P, Omar N, Van Mierlo J. Lithium-ion batteries health prognosis considering aging conditions. *IEEE Trans Power Electron*. 2019;34(7):6834-6844.
53. Smith KA, Rahn CD, Wang C. Model-based electrochemical estimation of lithium-ion batteries. Paper presented at: 2008 IEEE International Conference on Control Applications; 2008.
54. Subramanian S, Johny MA, Malamal Neelanchery M, Ansari S. Self-discharge and voltage recovery in graphene supercapacitors. *IEEE Trans Power Electron*. 2018;33(12):10410-10418.
55. Li K, Wei F, Tseng KJ, Soong BH. A practical lithium-ion battery model for state of energy and voltage responses prediction incorporating temperature and ageing effects. *IEEE Trans Ind Electron*. 2018;65(8):6696-6708.
56. Xiao Y. Model-based virtual thermal sensors for lithium-ion battery in EV applications. *IEEE Trans Ind Electron*. 2015;62(5):3112-3122.
57. Ruiz V, Pfrang A, Kriston A, Omar N, van den Bossche P, Boon-Brett L. A review of international abuse testing standards and regulations for lithium ion batteries in electric and hybrid electric vehicles. *Renew Sustain Energy Rev*. 2018;81:1427-1452.
58. Antón JCÁ, Nieto PJG, Viejo CB, Vilán JAA. Support vector machines used to estimate the battery state of charge. *IEEE Trans Power Electron*. 2013;28(12):5919-5926.
59. Hoke A, Brissette A, Smith K, Pratt A, Maksimovic D. Accounting for lithium-ion battery degradation in electric vehicle charging optimization. *IEEE J Emerg Sel Top Power Electron*. 2014;2(3):691-700.
60. Sun F, Hu X, Zou Y, Li S. Adaptive unscented Kalman filtering for state of charge estimation of a lithium-ion battery for electric vehicles. *Energy*. 2011;36(5):3531-3540.
61. Watrin N, Ostermann H, Blunier B, Miraoui A. Multiphysical lithium-based battery model for use in state-of-charge determination. *IEEE Trans Veh Technol*. 2012;61(8):3420-3429.
62. Gu R, Malysz P, Yang H, Emadi A. On the suitability of electrochemical-based modeling for lithium-ion batteries. *IEEE Trans Transport Electrificat*. 2016;2(4):417-431.
63. Charkhgard M, Farrokhi M. State-of-charge estimation for lithium-ion batteries using neural networks and EKF. *IEEE Trans Ind Electron*. 2010;57(12):4178-4187.
64. Lee K, Dai M, Chuang C. Temperature-compensated model for lithium-ion polymer batteries with extended Kalman filter state-of-charge estimation for an implantable charger. *IEEE Trans Ind Electron*. 2018;65(1):589-596.
65. He H, Xiong R, Zhang X, Sun F, Fan J. State-of-charge estimation of the lithium-ion battery using an adaptive extended Kalman filter based on an improved Thevenin model. *IEEE Trans Veh Technol*. 2011;60(4):1461-1469.
66. Wu B, Chen B. Study the performance of battery models for hybrid electric vehicles. Paper presented at: 2014 IEEE/ASME 10th International Conference on Mechatronic and Embedded Systems and Applications (MESA); 2014.
67. Allam A, Onori S. An interconnected observer for concurrent estimation of bulk and surface concentration in the cathode

- and anode of a lithium-ion battery. *IEEE Trans Ind Electron.* 2018;65(9):7311-7321.
68. Cao Y, Kroeze RC, Krein PT. Multi-timescale parametric electrical battery model for use in dynamic electric vehicle simulations. *IEEE Trans Transport Electrificat.* 2016;2(4):432-442.
69. Huria T, Ceraolo M, Gazzarri J, Jackey R. High fidelity electrical model with thermal dependence for characterization and simulation of high power lithium battery cells. Paper presented at: 2012 IEEE International Electric Vehicle Conference; 2012.
70. Urban A, Seo D-H, Ceder G. Computational understanding of Li-ion batteries. *NPJ Comput Mater.* 2016;2:16002.
71. Murashko K, Pyrhönen J, Laurila L. Three-dimensional thermal model of a lithium ion battery for hybrid Mobile working machines: determination of the model parameters in a pouch cell. *IEEE Trans Energy Convers.* 2013;28(2):335-343.
72. Park K, Choi Y, Choi WJ, Ryu HY, Kim H. LSTM-based battery remaining useful life prediction with multi-channel charging profiles. *IEEE Access.* 2020;8:20786-20798.
73. Crocioni G, Pau D, Delorme JM, Gruosso G. Li-ion batteries parameter estimation with tiny neural networks embedded on intelligent IoT microcontrollers. *IEEE Access.* 2020;8:122135-122146.

How to cite this article: Bairwa BL, Pareek K, Hampanavar Sk. Investigation on lithium ion battery equivalent circuit models for dynamic load profiles. *Energy Storage.* 2021;3:e231. <https://doi.org/10.1002/est2.231>